JIRRS
Journal International Review of Research Studies

Received: 28/06/2026 - **Accepted:** 23/07/2026
Vol: 01.10
DOI: 10.66104/xf9zhd03
Pages: 1-37

Screening-Level Operational Comparison of Commercial Sulfuric Acid Dosage and Measured ORP–pH Regimes during Atmospheric Leaching of a Ferruginous Nickel Laterite

Antonio Clareti Pereira, PhD
PhD in Chemical Engineering
University of São Paulo (USP)
Belo Horizonte, Minas Gerais, Brazil
E-mail: claretipereira@gmail.com
ORCID: https://orcid.org/0000-0001-8115-4279

Abstract

Atmospheric sulfuric acid leaching of ferruginous nickel laterites requires balancing valuable-metal transfer, acid use, total Fe loading, reductant consumption, and residue mineralogy. This screening-level study compares eight tests (PQH01–PQH08) conducted at 94–98 °C with 96 wt.% commercial H_2SO_4 solution at 293.5–552.2 kg solution/t dry ore. Redox values are reported as measured oxidation–reduction potential (ORP) on the original instrumental scale. Because ORP, pH, acid dosage, solids concentration, agitation, and metallic-bar exposure varied simultaneously, responses are interpreted as operational associations and reported as final-PLS yields per unit dry ore mass, not extraction or recovery. At nearly identical mean acid dosages of 543.6 and 543.3 kg solution/t dry ore, the higher-ORP G3 pair was associated with approximately 89% lower specific bar loss, 38% lower total Fe loading, 43% lower Fe/Ni, and 39% lower Fe/Co than the lower-ORP G1 pair, without an important Ni or Co yield penalty. Final residues showed lower relative modal contributions from Mg-bearing silicates, while residual Ni was concentrated in Fe oxyhydroxides and Ni-bearing Si–Fe plasma. Mn oxides were below the automated-mineralogy reporting limit in all residues; this does not prove complete dissolution. The transferable contribution is a screening framework showing that prolonged metallic-bar reduction may impose substantial reductant and total-Fe penalties without proportional valuable-metal benefit.

Keywords: Nickel laterite; atmospheric leaching; commercial sulfuric acid; measured ORP; final-PLS yield.

Highlights

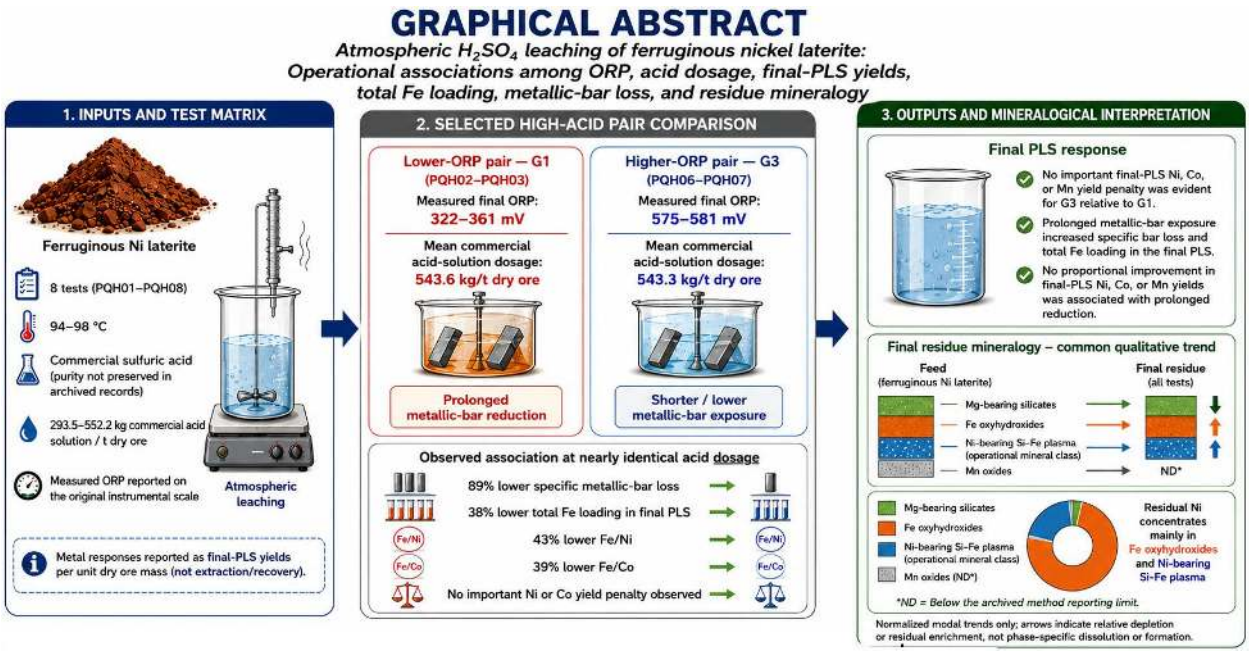
- Final-PLS yields were normalized to dry ore and distinguished from recovery.
- ORP values were retained on the original instrumental measurement scale.
- The higher-ORP operational bundle was associated with lower bar loss and total Fe loading.
- No major Ni or Co yield penalty was evident for the higher-ORP pair.

JIRRS
Journal International Review of Research Studies

Received: 28/06/2026 - **Accepted:** 23/07/2026
Vol: 01.10
DOI: 10.66104/xf9zhd03
Pages: 1-37

- Residual Ni was concentrated in Fe oxyhydroxides and Ni-bearing Si–Fe plasma.

Graphical abstract



Graphical abstract note. The diagram summarizes observed screening-level associations; final-PLS yield is not recovery, and no validated ORP or acid operating window is claimed.

1. Introduction

1.1. Strategic and processing context

Nickel laterites constitute a major resource base for the long-term supply of Ni and Co, but their processing is complicated by mineralogical heterogeneity, variable weathering profiles, low grades, and the intimate association of valuable metals with Fe- and Mn-bearing phases. Nickel remains essential to stainless steels and high-performance alloys, while the battery sector has increased the strategic importance of Co and battery-grade Ni intermediates. Recent reviews identify lateritic resources as central to future supply and emphasize lower reagent consumption, improved selectivity, and improved management of Fe-rich residues and liquors (Acquah et al., 2026; Caetano et al., 2025; Chi et al., 2026; Msumange et al., 2026; Mweene et al., 2024; Pandey et al., 2023; Stanković et al., 2020, 2022; Whittington & Muir, 2000).

JIRRS
Journal International Review of Research Studies
Received: 28/06/2026 - **Accepted:** 23/07/2026
Vol: 01.10
DOI: 10.66104/xf9zhd03
Pages: 1-37

Commercial and emerging laterite flowsheets include pressure acid leaching, atmospheric acid leaching, reduction roasting followed by leaching, heap and vat systems, chloride and nitrate media, hybrid hydrometallurgical routes, and biological processing. The suitability of each route depends on ore type, mineral deportment, energy demand, acid consumption, residue behavior, and downstream purification requirements. Alternative approaches include mechanical activation, thermal and microwave pretreatment, combined hydrometallurgical schemes, selective precipitation, and biological reduction or oxidation (Abdollahi et al., 2024; Acquah et al., 2025, 2026; de Alvarenga Oliveira et al., 2021; Dong et al., 2023; Hosseini Nasab et al., 2021; Johnson et al., 2021; Li et al., 2023; Prameswara et al., 2024; Ribeiro et al., 2021; Stanković et al., 2024; Tyassena et al., 2026; McDonald & Whittington, 2008).

1.2. Atmospheric leaching and the final-liquor selectivity problem

Atmospheric sulfuric acid leaching avoids the capital intensity of high-pressure systems but may require high acid dosages and long residence times. Conditions that release Ni from Fe-rich or poorly crystalline hosts can also increase the transfer of Fe, Al, Mg, and Mn to solution. The resulting PLS may require extensive neutralization and impurity removal. Studies on iron-rich laterites have shown that Ni response and Fe loading vary with acid dosage, temperature, time, and mineralogy, and that the highest Ni response does not necessarily represent the best process condition (da Silva Ribeiro et al., 2025; Hosseini Nasab et al., 2020; Ma et al., 2026; Pereira, 2026b; Prasetya et al., 2025; Santos et al., 2021).

The Fe penalty continues downstream because Fe removal can require neutralization, hydrolysis, phosphate precipitation, or other purification steps that increase chemical demand and solid generation (Boafo et al., 2026; Hosseini Nasab et al., 2022; Ma et al., 2026). The reactivity of Fe oxides and oxyhydroxides is sensitive to crystallinity, structural substitution, thermal history, and solution chemistry (Gontijo et al., 2020). Nitric acid, hydrochloric acid, ammonium hydrogen sulfate, mixed organic–sulfuric acid systems, $FeCl_3$-bearing solutions, roasting, microwave-assisted leaching, Taguchi optimization, and reduced-ore treatment provide useful comparisons (Hussaini et al., 2025; Khan et al., 2026;

JIRRS
Journal International Review of Research Studies
Received: 28/06/2026 - **Accepted:** 23/07/2026
Vol: 01.10
DOI: 10.66104/xf9zhd03
Pages: 1-37

Shayakhmetova et al., 2025; Wang et al., 2024; Yunita & Mubarok, 2021; Zablotskaya et al., 2022; Zhang et al., 2020).

1.3. Mineralogical controls and redox–pH coupling

In limonitic and ferruginous laterites, Ni may occur in goethite and related Fe oxyhydroxides, poorly crystalline Fe–Si domains, and subordinate Mg-bearing phyllosilicates. Co may occur in Fe-rich phases but is commonly enriched in Mn oxides and mixed Co–Mn oxyhydroxides. These associations control the sequence of metal release and impurity transfer, making phase-specific deportment and automated mineralogy valuable interpretive tools (Araujo et al., 2026; Domènech et al., 2022; Ziwa et al., 2021). Mechanical activation can increase accessibility, and the responses of limonitic and saprolitic materials differ because their dominant hosts and acid-consuming gangue phases differ (Acquah et al., 2026; Kang et al., 2026; Pereira, 2026a).

Reductive dissolution is coupled to proton availability. Simplified reactions for MnO_2 and goethite are shown below. The measured potential values are interpreted as operational ORP rather than thermodynamic Eh because the project sheets did not specify the reference-electrode scale or a conversion to the standard hydrogen electrode.

$$MnO_2 + 4H^+ + 2e^- \rightarrow Mn^{2+} + 2H_2O \quad (1)$$

$$FeOOH + 3H^+ + e^- \rightarrow Fe^{2+} + 2H_2O \quad (2)$$

These reactions illustrate why ORP and pH must be interpreted jointly. General redox geochemistry and coupled Fe–Mn reaction studies likewise emphasize dynamic interactions among mineral surfaces, dissolved species, electron donors, and proton-consuming reactions (Bafghi et al., 2008; Biswas et al., 2021; Huang & Zhang, 2020). Mn oxides are structurally diverse and important Co hosts; their response depends on structure, substitution, particle size, the identity of the reductant, and solution conditions (Boassen et al., 2026; Domènech et al., 2022). Reductive leaching and biological systems also show that Co-bearing Mn phases can be mobilized under reducing acidic conditions (Moro et al., 2023; Santos et al., 2020; Santos & Schippers, 2023).

JIRRS
Journal International Review of Research Studies

Received: 28/06/2026 - **Accepted:** 23/07/2026
Vol: 01.10
DOI: 10.66104/xf9zhd03
Pages: 1-37

Literature synthesis and positioning

Table 1 synthesizes the principal literature streams relevant to the present screening-level interpretation and clarifies how this study is positioned relative to established research on laterite leaching.

Table 1. Literature streams, established contributions, remaining limitations, and positioning of the present study

Literature stream	Established contribution	Remaining limitation	Position of this study
Laterite mineralogy and acid processing	Mineral hosts, ore-zone variability, and acid-leaching mechanisms are well established (Whittington & Muir, 2000; McDonald & Whittington, 2008).	Mineralogy and operating conditions vary strongly among deposits; numerical conditions are not directly transferable.	Uses feed and residue mineralogy to interpret an ore-specific campaign without claiming universal kinetics.
Atmospheric H_2SO_4 leaching and selectivity	Ni and Co transfer depends on acid dosage, temperature, time, and Fe-rich hosts (Hosseini Nasab et al., 2020; da Silva Ribeiro et al., 2025; Prasetya et al., 2025).	High Ni response can coincide with high Fe loading and incomplete process selectivity.	Reports final-PLS yield and total Fe loading rather than unsupported overall recovery.
Fe control and downstream purification	Fe precipitation and purification can increase reagent use and cause valuable-metal losses (Wang et al., 2011; Hosseini Nasab et al., 2022; Ma et al., 2026).	The Fe source is often not partitioned between ore dissolution, reductant corrosion, and secondary reactions.	Treats Fe as total final-PLS loading and provides an upper-bound bar-contribution screen.
Reductive Mn/Co mobilization and ORP	Acidic reduction can mobilize Mn- and Co-bearing phases, including with metallic Fe (Bafghi et al., 2008; Moro et al., 2023).	Measured slurry ORP is a mixed operational signal, not thermodynamic Eh without a known reference scale and speciation.	Interprets measured ORP as part of an operational bundle with pH and bar exposure.

JIRRS
Journal International Review of Research Studies
Received: 28/06/2026 - **Accepted:** 23/07/2026
Vol: 01.10
DOI: 10.66104/xf9zhd03
Pages: 1-37

Literature stream	Established contribution	Remaining limitation	Position of this study
Automated mineralogy and Ni deportment	QEMSCAN/SEM–EDS can identify modal mineralogy and Ni-host redistribution (Domènech et al., 2022; Araujo et al., 2026).	Normalized modal changes do not provide mass-balanced phase dissolution.	Uses only qualitative terms: modal depletion, persistence, and residual enrichment.

Note. The table distinguishes established scientific knowledge from the narrower, campaign-specific contribution of the present screening-level analysis.

1.4. Objective and scope

The objective was to perform a screening-level operational comparison of an atmospheric-leaching campaign by relating the dry-basis dosage of 96 wt.% commercial H_2SO_4 solution, observed ORP–pH trajectories, metallic-iron-bar exposure and consumption, final-PLS yields per unit dry ore mass, total Fe loading, and final-residue mineralogy. The study does not claim independent causal effects of acid dosage, measured ORP, or pH; it does not determine an optimum acid split between size fractions; and it does not report extraction or recovery because complete stream balances were unavailable. The primary comparison is between the G1 and G3 approximate operational pairs, which had comparable commercial-acid dosages but different bundled ORP–pH and bar-exposure conditions. Measured ORP is therefore treated as a descriptor of the operational regime rather than as an independently controlled variable.

2. Materials and Methods

2.1. Ore sample, preparation, and classification

A ferruginous nickel laterite from Goiás, central Brazil, was homogenized and classified at 100 mesh (approximately 150 μm) into a retained fraction (+100 mesh) and a passing fraction (−100 mesh). The project used the internal descriptors SAPSIL, SAPMG, and SAPFE for siliceous, Mg-bearing, and Fe-rich lateritic material classes, respectively; these are operational project categories rather than formal stratigraphic units. The classification record indicated nominal dry-mass recoveries of 60 wt.% in the +100 mesh

JIRRS
Journal International Review of Research Studies
Received: 28/06/2026 - **Accepted:** 23/07/2026
Vol: 01.10
DOI: 10.66104/xf9zhd03
Pages: 1-37

fraction and 40 wt.% in the −100 mesh fraction. This fixed 60:40 split was used to reconstruct the reference bulk-feed chemistry and mineralogy; the actual as-weighed test charges are reported separately in Table 4. The measured moisture content was 5.36 wt.%; dry ore mass was taken as 94.64% of the corresponding as-weighed ore mass. All ore-normalized final-PLS yields, acid-solution dosages, specific bar losses, and recovered-solids ratios were recalculated using moisture-corrected dry ore mass. Commercial sulfuric acid containing 96 wt.% H_2SO_4 was used. Dosage values refer to the mass of commercial solution per tonne of dry ore; the pure-H_2SO_4-equivalent dosage is obtained by multiplying by 0.96.

2.2. Chemical characterization of the size fractions

Table 2 reports the bulk chemical compositions measured for the retained and passing fractions.

Table 2. Chemical composition of the +100 and −100 mesh fractions (wt.%)

Component	+100 mesh	−100 mesh
Ni	1.078	1.005
Co	0.044	0.053
Fe	33.534	42.884
Mg	2.679	1.610
Mn	0.605	0.698
Si	13.315	7.859
Cr	1.865	1.081
Al	0.964	0.939
Ca	0.068	0.065
Zn	0.025	0.020
Loss on ignition	9.113	10.142

Note. Values reproduce the analytical basis of the original experimental campaign. Cu was approximately 0.01 wt.% in both fractions. All subsequent ore-normalized inventories and process responses were calculated using moisture-corrected dry ore masses. Source: Authors' compilation from the original analytical records.

The fractions had similar Ni grades, whereas the −100 mesh fraction contained more Fe and less Mg and Si. Thus, size classification changed the distribution of Ni among host phases rather than simply producing a high-Ni fraction.

2.3. Automated mineralogy and Ni deportment

Polished particle sections of the +100 and −100 mesh fractions were analyzed by QEMSCAN® automated mineralogy and scanning electron microscopy coupled with

JIRRS
Journal International Review of Research Studies
Received: 28/06/2026 - **Accepted:** 23/07/2026
Vol: 01.10
DOI: 10.66104/xf9zhd03
Pages: 1-37

energy-dispersive X-ray spectroscopy (SEM–EDS). QEMSCAN was used to quantify modal mineral composition and Ni deportment, while SEM–EDS analyses of representative phases supported and refined the project-specific mineral classification database. Samples were prepared and analyzed using the same project laboratory workflow, permitting internally consistent comparison among feed fractions and final residues.

Mineralogical interpretation emphasizes comparative behavior over certifying the abundance of trace phases, treating minor phases semiquantitatively. This is crucial for phases affected by low modal abundance or particle segregation, such as chromite, smectite, talc, Ti–Fe oxides, and spinels.

Mineral classification used the QEMSCAN mineral database and SEM–EDS compositions. Similar or unresolved phases were grouped; vermiculite and chlorite were combined due to unreliable separation. Minor Mn phases were grouped as Mn-oxides; hollandite was a Ba-rich, Ni-poor Mn oxide, while asbolane contained Co and Ni.

The Ni-bearing Si–Fe plasma is an automated-mineralogy class, representing amorphous or poorly crystalline Si-rich weathering areas with some Fe, Al, and Mg, formed from altered primary silicates like olivine, serpentine, and clays. It does not refer to a specific mineral. Complete modal compositions for both size fractions are in Table 3.

Table 3 presents the modal mineralogy used to interpret the contrasting mineral-host assemblages.

Table 3. Modal mineralogical composition of the +100 and −100 mesh fractions (wt.%)

Mineral phase or group	+100 mesh	−100 mesh
Quartz	9.25	1.39
Vermiculite/chlorite	13.94	3.82
Serpentine	4.88	1.18
Smectite	0.14	0.07
Phlogopite	0.97	0.39
Kaolinite	0.27	0.22
Talc	0.20	0.04
Other Fe–Mg silicates	1.55	1.78
Altered Fe–Mg silicates	4.51	2.35
Ni-bearing Si–Fe plasma	23.20	14.45

JIRRS
Journal International Review of Research Studies
Received: 28/06/2026 - **Accepted:** 23/07/2026
Vol: 01.10
DOI: 10.66104/xf9zhd03
Pages: 1-37

Mineral phase or group	+100 mesh	−100 mesh
Fe oxyhydroxides	27.66	69.43
Chromite	10.38	3.18
Mn oxides	1.07	0.78
Ti–Fe oxides	0.07	0.07
Spinels	0.06	0.09
Other phases	1.85	0.76

Source: Authors' compilation from the automated-mineralogy results generated during the experimental campaign.

The two size fractions showed markedly different mineralogical compositions. The −100 mesh fraction was dominated by Fe oxyhydroxides, which accounted for 69.43 wt.%, compared with 27.66 wt.% in the +100 mesh fraction. Conversely, the +100 mesh fraction contained larger proportions of quartz, vermiculite/chlorite, serpentine, altered Fe–Mg silicates, Ni-bearing Si–Fe plasma, chromite, and Mn oxides. Vermiculite/chlorite plus serpentine represented 18.82 wt.% of the +100 mesh fraction but only 5.00 wt.% of the −100 mesh fraction. These results show that size classification did not substantially concentrate Ni into a single fraction; instead, it altered the relative distribution of the mineral hosts in which Ni occurred.

The Ni-bearing Si–Fe plasma represented 23.20 wt.% of the +100 mesh fraction and 14.45 wt.% of the −100 mesh fraction. Its higher abundance in the coarse fraction was attributed to its frequent association with residual and altered phyllosilicates. The markedly higher Fe-oxyhydroxide abundance in the fine fraction indicates preferential concentration of the ferruginous limonitic matrix in the material passing 100 mesh.

SEM–EDS measurements generated during the campaign indicated average Ni contents of approximately 1.0 wt.% in Fe oxyhydroxides and 1.5 wt.% in the Si–Fe plasma. Average Ni contents of approximately 1.8 wt.% in vermiculite and 1.2 wt.% in serpentine were also reported, whereas chlorite generally contained no detectable Ni. These phase-average compositions, together with modal mineral abundances, were used to estimate Ni deportment among the principal mineral groups.

JIRRS
Journal International Review of Research Studies
Received: 28/06/2026 - **Accepted:** 23/07/2026
Vol: 01.10
DOI: 10.66104/xf9zhd03
Pages: 1-37

Nickel deportment to each mineral group was estimated from modal abundance and phase-average Ni composition using the following relation:

$$D_{Ni,j}\ (\%) = 100\ [X_j\ C_{Ni,j} / \Sigma_k\ (X_k\ C_{Ni,k})]$$

where the calculated deportment is the percentage of mineralogically assigned Ni attributed to mineral group j, the modal abundance is expressed as the mass fraction of that group, and the phase Ni concentration is derived from the project SEM–EDS measurements.

Mineralogical results show Fe oxyhydroxides and Ni-bearing Si–Fe plasma as the main Ni hosts in both fractions. Phyllosilicates contributed more in the +100 mesh fraction, about 30% of its Ni. The coarse fraction's higher Mg-bearing phyllosilicates and the fine fraction's ferruginous Ni hosts explain plausible differences in apparent leaching behavior. However, modal and deportment data alone do not confirm intrinsic kinetic differences, as fractions were not leached separately under same conditions.

The QEMSCAN-derived chemistry matched bulk analyses overall, with larger differences for Fe and Cr. Chromite variability may reflect segregation during sample prep. Minor-phase values are semi-quantitative, but main conclusions focus on dominant minerals. The Ni-bearing Si–Fe plasma class is supported by modal data, SEM–EDS compositions, and mineralogy. Figure 1 combines composition, mineralogy, and Ni distribution, without implying reactivity. All feed and final-residue modal distributions used in the comparisons were normalized to 100%. Mineralogy provides a plausible explanation of process constraints but does not quantify intrinsic leachability of either size fraction or of any individual host phase.

JIRRS
Journal International Review of Research Studies

Received: 28/06/2026 - **Accepted:** 23/07/2026
Vol: 01.10
DOI: 10.66104/xf9zhd03
Pages: 1-37

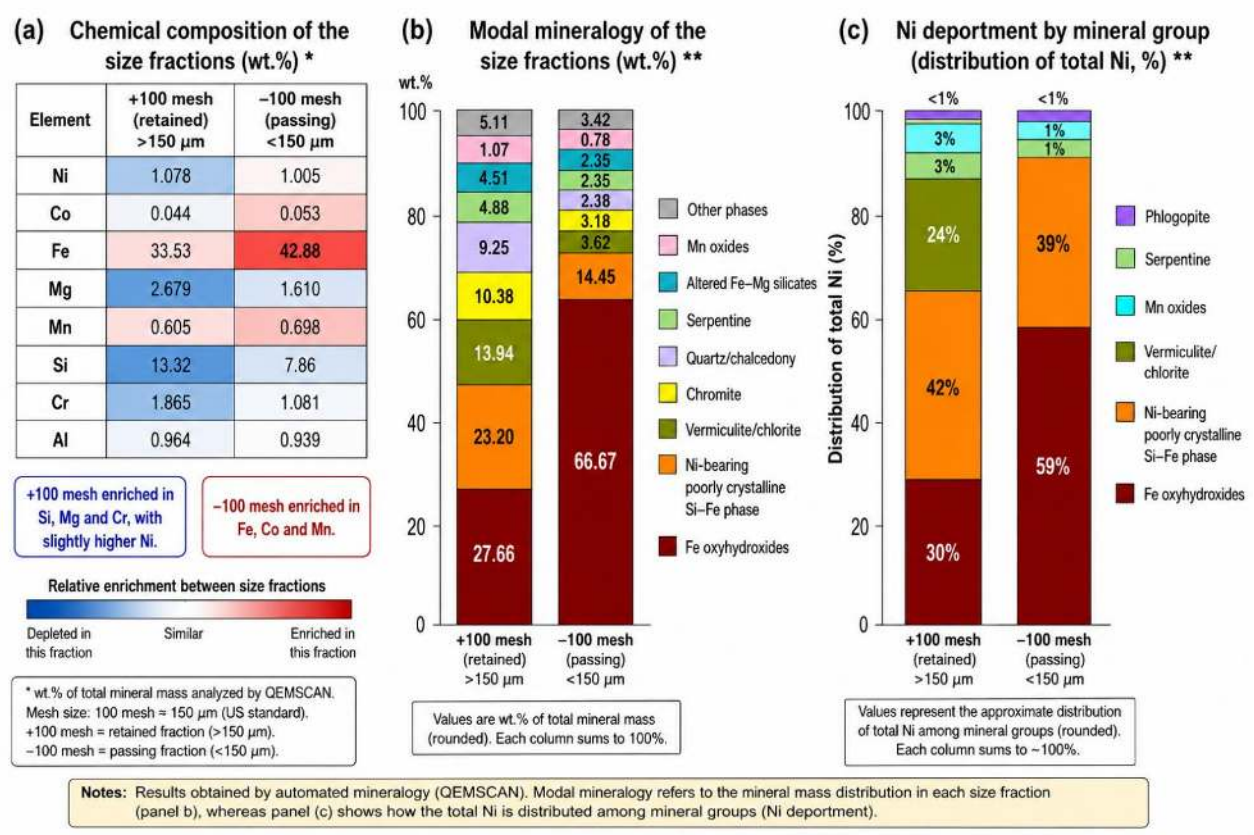


Figure 1. Chemical, modal-mineralogical, and Ni-deportment contrast between the +100 and −100 mesh fractions.

Note. The figure compares mineral abundance with Ni deportment and does not imply measured intrinsic reactivity. Source: Authors' compilation from Tables 1–2 and the Ni-deportment data generated during the campaign.

2.4. Test identification and experimental matrix

Table 4 summarizes the as-weighed charges, moisture-corrected dry ore masses, dry-basis dosages of 96 wt.% commercial H_2SO_4 solution, ORP–pH classifications, and metallic-bar losses for PQH01–PQH08.

Table 4. Global operating conditions of PQH01–PQH08 on as-weighed and dry-ore bases

Code	Ore, as weighed (g)	Dry ore (g)	96 wt.% commercial H_2SO_4 solution mass (g)	Commercial H_2SO_4 solution dosage (kg/t dry ore)	Operational ORP–pH group	Final ORP (mV)	Final pH	Bar loss (g)	Specific bar loss (kg/t dry ore)
PQH01	391.98	370.97	160.02	431.4	Lower ORP	317	1.88	25.03	67.5

JIRRS
Journal International Review of Research Studies
Received: 28/06/2026 - **Accepted:** 23/07/2026
Vol: 01.10
DOI: 10.66104/xf9zhd03
Pages: 1-37

Code	Ore, as weighed (g)	Dry ore (g)	96 wt.% commercial H_2SO_4 solution mass (g)	Commercial H_2SO_4 solution dosage (kg/t dry ore)	Operational ORP–pH group	Final ORP (mV)	Final pH	Bar loss (g)	Specific bar loss (kg/t dry ore)
PQH02	386.68	365.95	200.03	546.6	Lower ORP	361	1.70	38.57	105.4
PQH03	391.00	370.04	200.04	540.6	Lower ORP	322	1.88	38.84	105.0
PQH04	399.28	377.88	163.35	432.3	Higher ORP	552	0.82	3.81	10.1
PQH05	405.81	384.06	160.11	416.9	Higher ORP	564	1.09	3.81	9.9
PQH06	402.14	380.59	203.39	534.4	Higher ORP	581	0.58	4.71	12.4
PQH07	390.46	369.53	204.07	552.2	Higher ORP	575	0.81	3.78	10.2
PQH08	587.27	555.79	163.14	293.5	Higher ORP	558	0.78	3.62	6.5

Note. Ore masses recorded during the experiments are shown on an as-weighed basis. Dry ore masses were calculated based on a measured moisture content of 5.36 wt.%. Acid dosage refers to the mass of 96 wt.% commercial H_2SO_4 solution per tonne of dry ore; multiplication by 0.96 gives the pure-H_2SO_4-equivalent dosage. Specific metallic-bar loss is expressed per tonne of dry ore. ORP values are reported on the original instrumental scale because the project sheets did not specify the reference-electrode conversion. Source: Authors' calculations from the original test sheets.

PQH02–PQH03 and PQH06–PQH07 had nearly identical mean dry-basis dosages of 96 wt.% commercial H_2SO_4 solution of 543.6 and 543.3 kg/t dry ore, respectively, but clearly different observed ORP–pH trajectories. These n = 2 pairs form the principal basis for descriptive operational comparison and are not true replicates. PQH04–PQH05 form a second pair, with a mean commercial acid dosage of approximately 424.6 kg/t of dry ore. PQH01 and PQH08 are treated as individual exploratory conditions. Figure 2 locates all tests in commercial-acid-dosage versus measured final-ORP space and identifies the approximate operational pairs. The higher-ORP label denotes an operational bundle characterized by shorter metallic-bar exposure, lower bar loss, a different final-pH range, and a higher measured ORP endpoint; it must not be interpreted as independent electrochemical control. Recorded bar-exposure information is summarized in Supplementary Table S3.

JIRRS
Journal International Review of Research Studies
Received: 28/06/2026 - **Accepted:** 23/07/2026
Vol: 01.10
DOI: 10.66104/xf9zhd03
Pages: 1-37

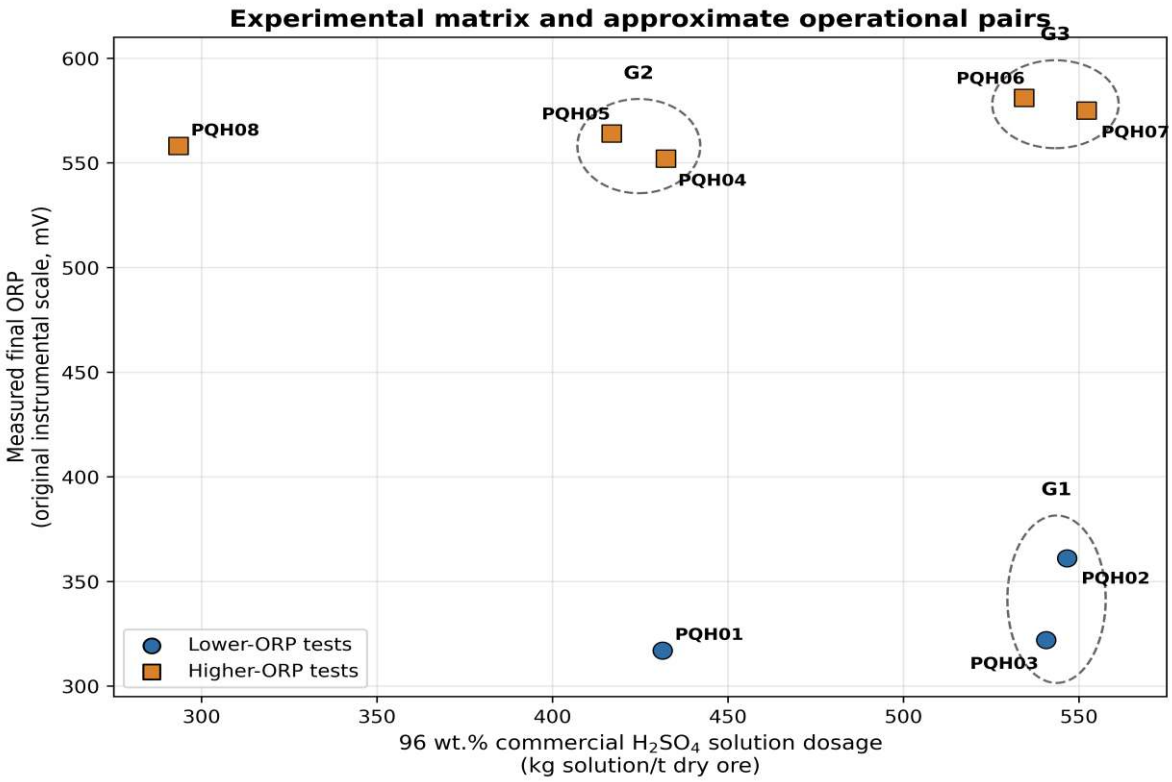


Figure 2. Experimental matrix plotted as dry-basis dosage of 96 wt.% commercial H_2SO_4 solution versus measured final ORP. Note. G1–G3 indicate approximate operational pairs, not true replicates or statistical treatment blocks. The plotted dosage is the mass of commercial acid solution per tonne of dry ore. Source: Authors' calculations from Table 4.

2.5. Atmospheric leaching procedure

Each test comprised two operational stages within one global experiment. In stage 1, the +100 mesh fraction was mixed with water and sulfuric acid and leached for 2 h at approximately 94–98 °C. An intermediate slurry sample was removed, filtered, washed, dried, and chemically analyzed. The −100 mesh fraction and the remaining water and acid specified in the original test sheet were then added. Agitation was adjusted according to the individual sheet. Metallic-iron bars were introduced during stage 2 as reductants; the exact alloy grade and carbon content were not specified in the test records. ORP, pH, and temperature were recorded periodically. The bars were removed after test-specific exposure periods, and the total test duration was approximately 7 h. The final slurry was filtered and washed, and the final PLS and residue were analyzed.

JIRRS
Journal International Review of Research Studies
Received: 28/06/2026 - **Accepted:** 23/07/2026
Vol: 01.10
DOI: 10.66104/xf9zhd03
Pages: 1-37

The sequence is reported for traceability but was not a controlled acid-split experiment; consequently, no optimal stagewise acid distribution can be inferred. Figure 3 summarizes the experimental sequence and distinguishes the intermediate analytical sample from the final PLS and residue response streams.

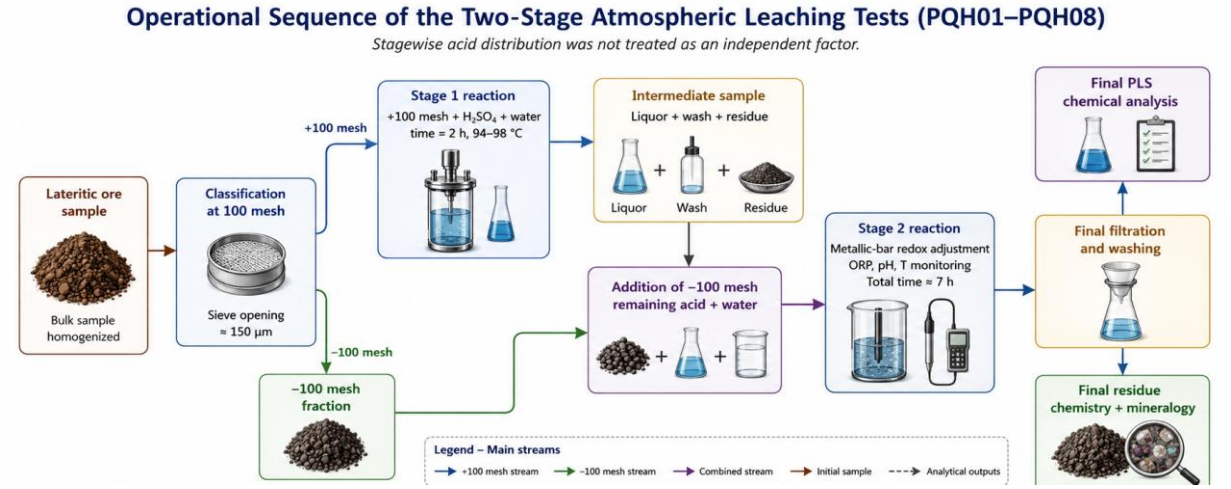


Figure 3. Experimental sequence used in the global atmospheric-leaching campaign. Source: Authors' schematic based on the original operating records.

2.6. Analytical data provenance and process measurements

The analytical program covered the +100 and −100 mesh feed fractions, sulfuric acid leach liquors, wash solutions, intermediate residues, and final dried residues. Liquid samples were analyzed under laboratory procedure PROPL21 by inductively coupled plasma (ICP) spectrometric analysis. Feed and residue samples were prepared by alkaline fusion with Na_2CO_3 and $Na_2B_4O_7$ and analyzed by plasma spectrometry under procedure PROPL11; Cu was determined after aqua-regia solubilization by atomic absorption under PROAA15, and loss on ignition was determined under PROVU01 by calcination for 2 h at 1000 °C followed by gravimetry. The comparison focuses on Ni, Co, Mn, Fe, Mg, Al, Cr, Si, and Zn because these elements are most relevant to valuable-metal transfer, acid-consuming gangue behavior, total Fe loading, and residue interpretation.

Liquor and wash solution aliquots submitted for chemical analysis were diluted fivefold with deionized water adjusted to pH 1.0. Concentrations were subsequently

JIRRS
Journal International Review of Research Studies
Received: 28/06/2026 - **Accepted:** 23/07/2026
Vol: 01.10
DOI: 10.66104/xf9zhd03
Pages: 1-37

corrected using the recorded dilution factor. The campaign certificates reported a method reporting limit of 0.01 µg/mL for the analyzed liquid aliquot. For fivefold-diluted samples, the corresponding process-solution reporting limit was 0.05 µg/mL. The concentration in the original process solution was obtained from:

$$C_{i,original} = D \times C_{i,diluted}$$

where the corrected concentration refers to element i in the original process solution, the measured concentration refers to the fivefold-diluted aliquot, and D is the dilution factor, nominally equal to 5. When the project sheets already contained dilution-corrected concentrations, those corrected values were used directly. The available laboratory method register for PROPL11 reported the following method-level limits (wt.%), which are used as reporting thresholds rather than independently reconstructed campaign-specific detection limits: Al 0.074, Ca 0.065, Co 0.028, Cr 0.204, Cu 0.010, Fe 0.369, Mg 0.169, Mn 0.053, Ni 0.178, Si 0.183, Zn 0.010, and loss on ignition 0.108.

At the end of each test, the slurry was filtered to separate the final pregnant leach solution (PLS). The residue was subsequently washed using deionized water at approximately 70 °C, and the resulting wash stream was recorded; final-wash chemistry was not available for the PQH01–PQH08 comparison. The original procedure specified approximately 4500 g of wash water for the final residue. The washed residue was weighed in its wet and dry states and divided, where sufficient material was available, for chemical and mineralogical characterization.

The experimental records include measured or dilution-corrected concentrations for the intermediate liquor, intermediate wash, and final PLS, together with intermediate- and final-residue masses and selected solid analyses. Final-wash chemistry, solution retained in the filter cake, and unrecorded process losses were not available for a closed balance. Supplementary Table S1 provides a test-by-test data-completeness matrix. Consequently, the study reports final-PLS yields per unit mass of dry ore and does not present these values as extraction, recovery, or a closed-stream metallurgical balance.

JIRRS
Journal International Review of Research Studies
Received: 28/06/2026 - **Accepted:** 23/07/2026
Vol: 01.10
DOI: 10.66104/xf9zhd03
Pages: 1-37

The analytical certificates identify the laboratory procedure codes, sample identities, dilution factors, units, and reporting limits; these details are consolidated in Supplementary Table S4. The instrument make/model and the campaign-specific duplicate, certified-reference-material, and recovery summaries were not included with the PQH analytical package used for this manuscript. Therefore, no independent estimate of analytical precision or accuracy is assigned beyond the issued laboratory results. This limitation affects absolute certification more than the internally consistent screening comparison, but it remains explicitly acknowledged.

Numerical values preceded by a less-than sign were retained as below-reporting-limit results and were not replaced by zero in qualitative comparisons. No below-reporting-limit final-PLS concentration was used to calculate the Ni, Co, Mn, or total-Fe yields reported in the main comparison. Where a numerical treatment of a below-limit solid result was necessary, the applicable reporting limit and assumption are stated; Mn-oxide values of 0.00 in the automated-mineralogy table are interpreted only as below the method reporting capability, not as proof of complete dissolution.

The process variables recorded during the campaign included slurry mass, slurry density, liquor mass, liquor density, calculated or measured volume, pH, redox potential, temperature, free acidity, and, in some records, viscosity. During the second leaching stage, pH and redox potential were measured at approximately 15-min intervals after insertion of the metallic bars. The work plan also required recording the initial and final masses of the bars to quantify metallic-material loss.

The test records referred to the redox measurements as “Eh,” but no conversion from the measurement reference electrode to the standard hydrogen electrode was included. The redox variable is therefore reported throughout as measured oxidation–reduction potential (ORP), in millivolts on the original instrumental scale, rather than as thermodynamic Eh. No standard-electrode conversion was applied.

Measured ORP in a hot, concentrated slurry is an operational mixed potential influenced by the unknown reference-electrode offset, temperature, acid concentration,

JIRRS
Journal International Review of Research Studies
Received: 28/06/2026 - **Accepted:** 23/07/2026
Vol: 01.10
DOI: 10.66104/xf9zhd03
Pages: 1-37

dissolved Fe^{2+}/Fe^{3+} and other redox couples, gas exchange, mineral and metallic surfaces, solids contact, and electrode polarization. Consequently, the recorded values cannot be mapped directly onto thermodynamic mineral-stability fields. PQH01–PQH03 reached final measured ORP values of approximately 317–361 mV, whereas PQH04–PQH08 reached approximately 552–581 mV on the original scale. These are empirical endpoint classifications for this campaign. Because pH, temperature, acid availability, solids concentration, bar-contact time, and ORP varied simultaneously, ORP is not interpreted as an independently controlled causal variable.

The experimental procedure required pH and ORP monitoring during the tests. Measurements were made in reaction slurry, separated liquor, or wash solution, depending on the sampling point. Because these matrices differ in temperature, gas exchange, solids content, equilibration time, and electrode geometry, reactor-slurry and separated-solution readings are not assumed to represent identical electrochemical states and are compared only within the same measurement matrix.

Recorded slurry and liquor masses and densities were used to reconstruct operational process volumes. Density-derived volumes are treated as campaign measurements and are reported with precision consistent with the original test sheets.

Free acidity was recorded for selected leach liquors and wash solutions. Because the reporting basis in the project sheets was not explicitly defined, free-acidity values are used only as qualitative indicators of residual proton availability and are excluded from quantitative comparisons, regression analyses, mass balances, and operating-window calculations.

Conclusions are based on internally consistent differences among tests and on responses substantially larger than observed within-pair variation. The investigation is a screening-level operational comparison, not a causal optimization study or a universally transferable ORP–pH operating window. Future validation should include a known ORP reference scale, independently controlled pH and ORP, Fe^{2+}/Fe^{3+} speciation, quantitative free-acidity determination, blank bar-corrosion tests, complete analysis of every liquid and solid stream, and propagated measurement uncertainty.

JIRRS
Journal International Review of Research Studies
Received: 28/06/2026 - **Accepted:** 23/07/2026
Vol: 01.10
DOI: 10.66104/xf9zhd03
Pages: 1-37

2.7. Final-PLS yield and selectivity calculations

The volume of final PLS was calculated from the recorded liquor mass and density:

$$V_{PLS} = m_{PLS} / \rho_{PLS} \quad (3)$$

The mass of element i in the final PLS and its final-PLS yield per unit dry ore mass were calculated as:

$$m_{i,PLS} = C_{i,PLS} \times V_{PLS} \quad (4)$$
$$Y_{i,PLS} = m_{i,PLS} / m_{ore,dry} \quad (5)$$

Final-PLS yields are reported as grams of element in the final PLS per kilogram of dry ore. This metric does not include the intermediate liquor, intermediate wash, final wash, solution retained in solids, or unrecorded losses. It is therefore not equivalent to extraction, recovery, or a closed metallurgical balance. The fraction of the dry-feed Ni inventory present in the final PLS was calculated only as a descriptive inventory ratio.

$$F_{Ni,final\ PLS}\ (\%) = 100\ Y_{Ni,PLS} / C_{Ni,feed} \quad (6)$$

Selectivity ratios and specific metallic-bar loss were calculated as:

$$R_{Fe/Ni} = m_{Fe,PLS} / m_{Ni,PLS}; \quad R_{Fe/Co} = m_{Fe,PLS} / m_{Co,PLS} \quad (7)$$
$$C_{bar} = 1000\ [m_{bar,initial} - m_{bar,final}] / m_{ore,dry} \quad (8)$$

Because the bars could corrode, form scale, retain precipitates, or contribute solids, bar mass loss is interpreted as specific metallic-material consumption and an upper-bound indicator of potential Fe addition. Total Fe loading in the final PLS cannot be separated into ore-derived and bar-derived contributions with the available data. A numerical upper-bound screen is provided in Supplementary Table S2.

2.8. Weighted feed and final-residue mineralogy

The classification mass recovery was nominally 60 wt.% for +100 mesh and 40 wt.% for −100 mesh, on a dry basis. Accordingly, the same fixed dry-mass-weighted feed mineralogy was used as the reference composition for PQH01–PQH08:

$$X_{j,feed} = 0.60\ X_{j,+100} + 0.40\ X_{j,-100} \quad (9)$$

The fixed 60:40 dry-mass-weighted feed and each final residue are compared as normalized modal distributions. No phase-specific dissolution percentages are reported because the intermediate residue was produced before addition of the fine fraction, was not

JIRRS
Journal International Review of Research Studies
Received: 28/06/2026 - **Accepted:** 23/07/2026
Vol: 01.10
DOI: 10.66104/xf9zhd03
Pages: 1-37

mineralogically characterized, and did not experience stage 2. Applying final-residue mineralogy to that intermediate solid would be structurally invalid. Changes are therefore described only as modal depletion, persistence, or residual enrichment.

2.9. Descriptive statistical treatment

The campaign was not a balanced factorial design and contained no true triplicates. PQH02–PQH03 (G1), PQH04–PQH05 (G2), and PQH06–PQH07 (G3) are treated as approximate operational pairs. Mean and relative percent difference (RPD) are used only to describe within-pair operational agreement:

$$\text{RPD}\ (\%) = 100\ |X_1 - X_2| \,/\, [(X_1 + X_2)/2] \quad (10)$$

With n = 2, standard deviations and coefficients of variation do not provide robust estimates of experimental variability. No null-hypothesis significance tests or causal multivariable models were applied. ORP and pH were correlated with acid dosage, solids concentration, agitation, and bar exposure; results are interpreted as associations with observed operational regimes.

3. Results and Discussion

3.1. Chemical and mineralogical contrast between size fractions

The fractions had similar Ni grades but different mineral assemblages. Relative to the +100 mesh fraction, the −100 mesh fraction contained more Fe, less Mg and Si, and Fe oxyhydroxides made up 69.43 wt.% instead of 27.66 wt.%. Coarse fractions had more vermiculite/chlorite, serpentine, altered Fe–Mg silicates, and Ni-bearing Si–Fe plasma. This reflects a silicate-rich coarse and limonitic fine fraction. Similar phase-dependent behavior has been observed, with Ni-bearing phyllosilicates responding early and Ni associated with Fe oxyhydroxides being mobilized with increasing Fe transfer (Araujo et al., 2026; Kang et al., 2026; Shayakhmetova et al., 2025).

The data support only a mineralogical inference that the +100 mesh fraction may be more acid-reactive. Intrinsic reactivity cannot be demonstrated because the fractions were not tested independently under identical conditions. Accordingly, the mineralogical contrast

JIRRS
Journal International Review of Research Studies
Received: 28/06/2026 - **Accepted:** 23/07/2026
Vol: 01.10
DOI: 10.66104/xf9zhd03
Pages: 1-37

is used to explain plausible constraints, not to assign intrinsic rate constants or phase-specific leachability.

3.2. Final-PLS yields and incomplete inventory closure

Table 5 presents the final-PLS yields recalculated per kilogram of dry ore, together with descriptive Ni-inventory and Fe-selectivity indicators.

Table 5. Final-PLS yields per unit dry ore mass and process-selectivity indicators

Test	Final PLS (mL)	Ni (g/kg dry ore)	Feed Ni in final PLS (%)	Co (g/kg dry ore)	Mn (g/kg dry ore)	Total Fe (g/kg dry ore)	Fe/Ni	Fe/Co
PQH01	884.76	3.494	33.3	0.248	3.012	105.8	30.3	426.5
PQH02	852.23	3.617	34.5	0.247	3.232	151.4	41.9	613.3
PQH03	820.49	3.572	34.1	0.242	3.002	148.3	41.5	613.6
PQH04	957.50	3.715	35.4	0.254	2.940	65.4	17.6	258.0
PQH05	900.40	3.669	35.0	0.248	2.822	69.7	19.0	280.5
PQH06	793.85	3.690	35.2	0.244	2.968	89.4	24.2	366.3
PQH07	860.58	4.145	39.5	0.259	3.037	97.9	23.6	378.7
PQH08	742.19	2.546	24.3	0.198	2.223	32.8	12.9	165.7

Source: Authors' calculations from the final-PLS analyses and feed compositions generated during the campaign.

Final-PLS Ni yield ranged from 2.546 to 4.145 g/kg dry ore, corresponding to approximately 24.3–39.5% of the calculated dry-feed Ni inventory. These descriptive inventory fractions confirm that final-PLS yield is not extraction or recovery because several liquid and retained-solution streams are excluded. PQH07 had the highest final-PLS Ni yield but also substantial total Fe loading. PQH08 had the lowest Fe/Ni ratio and total Fe loading, but it also had the lowest final-PLS Ni yield and a higher residual Ni grade. The principal operational trade-off was therefore between Ni transferred to the final PLS and total Fe carried by that solution. Figure 4 compares these dry-basis responses with the dosage of 96 wt.% commercial H_2SO_4 solution.

JIRRS
Journal International Review of Research Studies
Received: 28/06/2026 - **Accepted:** 23/07/2026
Vol: 01.10
DOI: 10.66104/xf9zhd03
Pages: 1-37

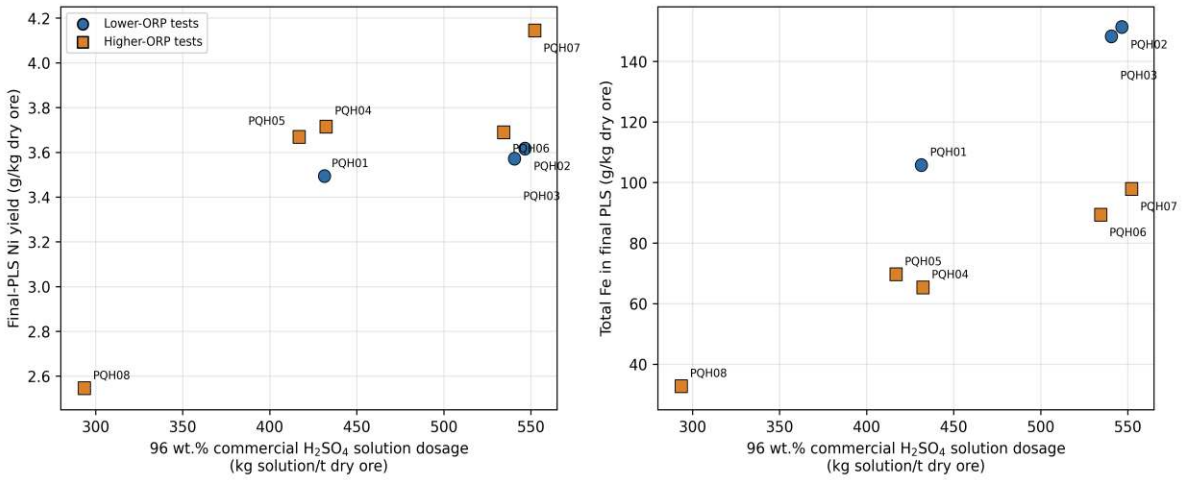


Figure 4. Final-PLS Ni yield and total Fe loading as functions of dry-basis dosage of 96 wt.% commercial H_2SO_4 solution. Note. Dosage values refer to commercial acid solution mass per tonne of dry ore. Source: Authors' calculations from Table 5.

3.3. Within-pair operational agreement

Table 6 summarizes pair means and RPD values used only to assess within-pair operational agreement.

Table 6. Descriptive within-pair agreement for G1–G3 on a dry-ore basis

Group	Response	Pair mean	RPD (%)
G1	Ni (g/kg dry ore)	3.595	1.24
G1	Co (g/kg dry ore)	0.245	2.12
G1	Mn (g/kg dry ore)	3.117	7.38
G1	Total Fe (g/kg dry ore)	149.9	2.08
G2	Ni (g/kg dry ore)	3.692	1.24
G2	Co (g/kg dry ore)	0.251	1.94
G2	Mn (g/kg dry ore)	2.881	4.05
G2	Total Fe (g/kg dry ore)	67.5	6.42
G3	Ni (g/kg dry ore)	3.917	11.63
G3	Co (g/kg dry ore)	0.251	5.75
G3	Mn (g/kg dry ore)	3.002	2.29
G3	Total Fe (g/kg dry ore)	93.7	9.08

Source: Authors' calculations from Tables 3–4.

G1 and G2 showed close within-pair agreement for the final PLS Ni and Co yields. G3 showed an Ni RPD of approximately 11.6%, which is larger than the difference in Ni yield

JIRRS
Journal International Review of Research Studies
Received: 28/06/2026 - **Accepted:** 23/07/2026
Vol: 01.10
DOI: 10.66104/xf9zhd03
Pages: 1-37

between the G1 and G3 pair means. Therefore, the data do not demonstrate that the higher-ORP regime increased Ni yield. The defensible interpretation is that there was no evidence of an important Ni or Co yield penalty, whereas differences in bar loss and total Fe loading were much larger than the observed within-pair variation. All pair means are therefore descriptive n = 2 summaries; no significance testing or population-level uncertainty is implied.

3.4. Observed ORP–pH trajectories

PQH01–PQH03 reached measured final ORP values of 317–361 mV on the original instrumental scale, while PQH04–PQH08 stabilized at 552–581 mV. The lower-ORP tests involved longer metallic-bar exposure, and in the higher-ORP tests, bars were removed after the initial potential drop, with ORP remaining stable. Final pH was higher in lower-ORP tests and lower in higher-ORP tests, preventing ORP and pH from being separated as independent variables. Figure 5 shows the time-resolved ORP trajectories with the two endpoint ranges labeled, without implying thermodynamic stability. The higher-ORP designation should therefore be read as shorthand for the combined shorter-bar-exposure, pH, and ORP operational bundle.

JIRRS
Journal International Review of Research Studies

Received: 28/06/2026 - **Accepted:** 23/07/2026
Vol: 01.10
DOI: 10.66104/xf9zhd03
Pages: 1-37

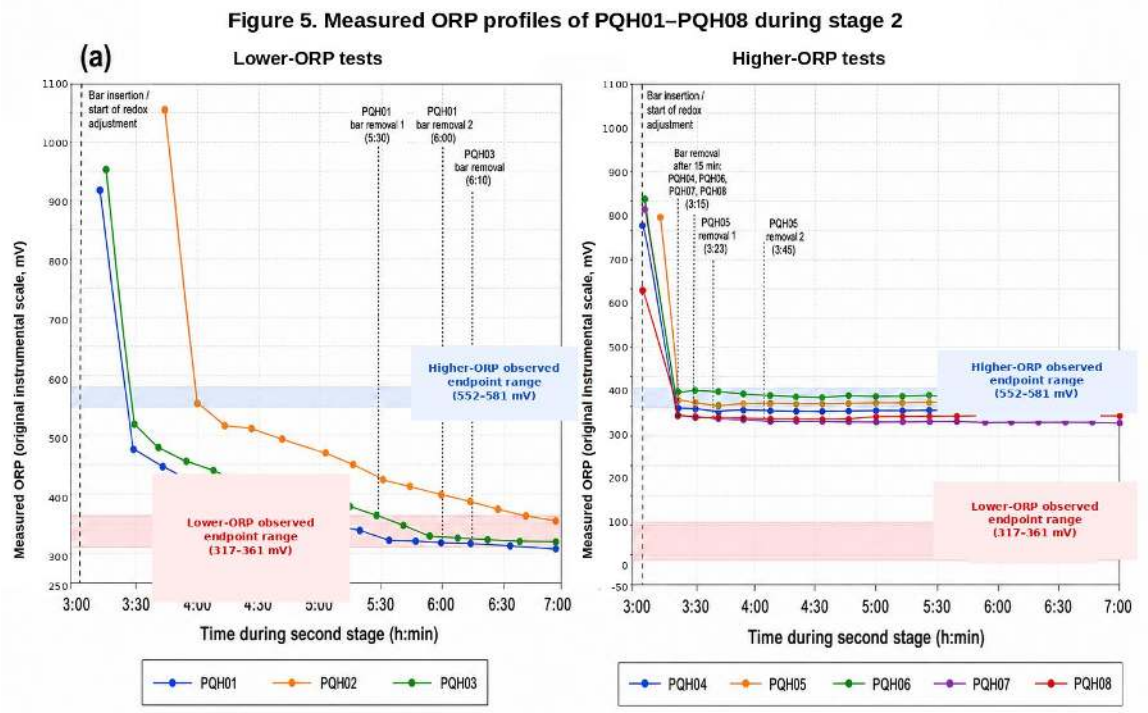


Figure 5. Measured ORP profiles during stage 2 for PQH01–PQH08, separated into lower-ORP and higher-ORP tests. Source: Authors' compilation from the original time-resolved redox records.

3.5. Comparable-acid lower-ORP versus higher-ORP operational pairs

Table 7 presents a direct screening-level comparison between the lower-ORP G1 and higher-ORP G3 operational pairs, which had nearly identical mean commercial-acid dosages but were not controlled replicates.

Table 7. Screening-level comparison of the comparable-acid G1 and G3 operational pairs on a dry-ore basis

Response	G1 mean	G3 mean	Difference in G3 vs G1 (%)	Interpretation
Specific bar loss (kg/t dry ore)	105.2	11.3	−89.3	Large operational decrease
Ni in final PLS (g/kg dry ore)	3.595	3.917	+9.0	Difference smaller than G3 pair variability
Co in final PLS (g/kg dry ore)	0.245	0.251	+2.9	No important penalty evident
Mn in final PLS (g/kg dry ore)	3.117	3.002	−3.7	Similar final-PLS yield
Total Fe in final PLS (g/kg dry ore)	149.9	93.7	−37.5	Large decrease in total Fe loading

JIRRS
Journal International Review of Research Studies
Received: 28/06/2026 - **Accepted:** 23/07/2026
Vol: 01.10
DOI: 10.66104/xf9zhd03
Pages: 1-37

Response	G1 mean	G3 mean	Difference in G3 vs G1 (%)	Interpretation
Fe/Ni (kg/kg)	41.7	23.9	−42.6	Improved process ratio
Fe/Co (kg/kg)	613.5	372.5	−39.3	Improved process ratio
Recovered-solids-to-dry-feed ratio (%)	85.1	82.5	−3.1	Similar process descriptor
Residual Ni (wt.%)	0.640	0.655	+2.3	Similar residual grade

Source: Authors' calculations from the approximate operational pairs.

Relative to G1, the G3 operational bundle was associated with approximately 89% lower specific metallic-bar loss, 38% lower total Fe loading, 43% lower Fe/Ni, and 39% lower Fe/Co. Final-PLS Co and Mn yields were similar. The approximately 9% higher mean Ni yield in G3 is not interpreted as an improvement because G3 itself had an Ni RPD of approximately 11.6%. Thus, Fe-loading and bar-loss differences were large relative to within-pair variation, whereas the Ni difference was not. Figure 6 displays the individual observations and pair means so that the limited n = 2 agreement remains visible.

JIRRS
Journal International Review of Research Studies
Received: 28/06/2026 - **Accepted:** 23/07/2026
Vol: 01.10
DOI: 10.66104/xf9zhd03
Pages: 1-37

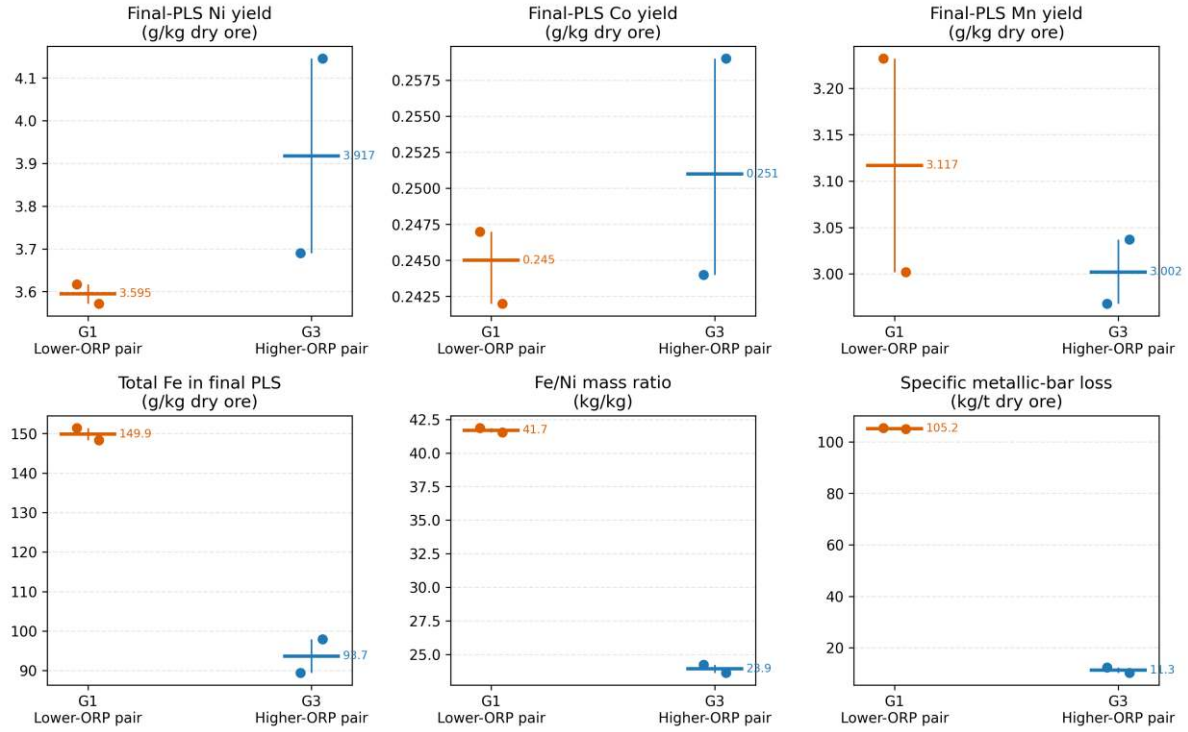


Figure 6. Individual responses and pair means for the comparable-acid lower-ORP G1 and higher-ORP G3 operational pairs. Note. Each pair contains only two tests and is not a true replicate block. Source: Authors' calculations from Table 7.

3.6. Metallic-bar consumption and total Fe loading

Specific metallic-bar loss ranged from 67.5 to 105.4 kg/t dry ore in PQH01–PQH03 and from 6.5 to 12.4 kg/t dry ore in PQH04–PQH08. Lower measured ORP occurred within the operational bundle that also involved prolonged bar exposure and substantially greater metallic-material consumption; ORP alone is not assigned causal responsibility. The work sheets designated the reductant as metallic iron, but the exact alloy grade was not reported. Assuming only as an upper bound that all lost bar mass was Fe and all of it entered the final PLS, bar loss could represent approximately 64–71% of the measured final-PLS Fe in PQH01–PQH03 and 10–20% in PQH04–PQH08 (Supplementary Table S2). This is not source apportionment because bar scale, precipitates, undissolved corrosion products, alloy constituents, and ore-derived Fe were not independently quantified. The valid response is therefore total Fe loading in the final PLS, not ore Fe dissolution.

JIRRS
Journal International Review of Research Studies
Received: 28/06/2026 - **Accepted:** 23/07/2026
Vol: 01.10
DOI: 10.66104/xf9zhd03
Pages: 1-37

Figure 7 integrates measured final ORP, specific metallic-bar loss, total Fe loading, and dry-basis dosage of 96 wt.% commercial H_2SO_4 solution without assigning independent causal effects to any single variable.

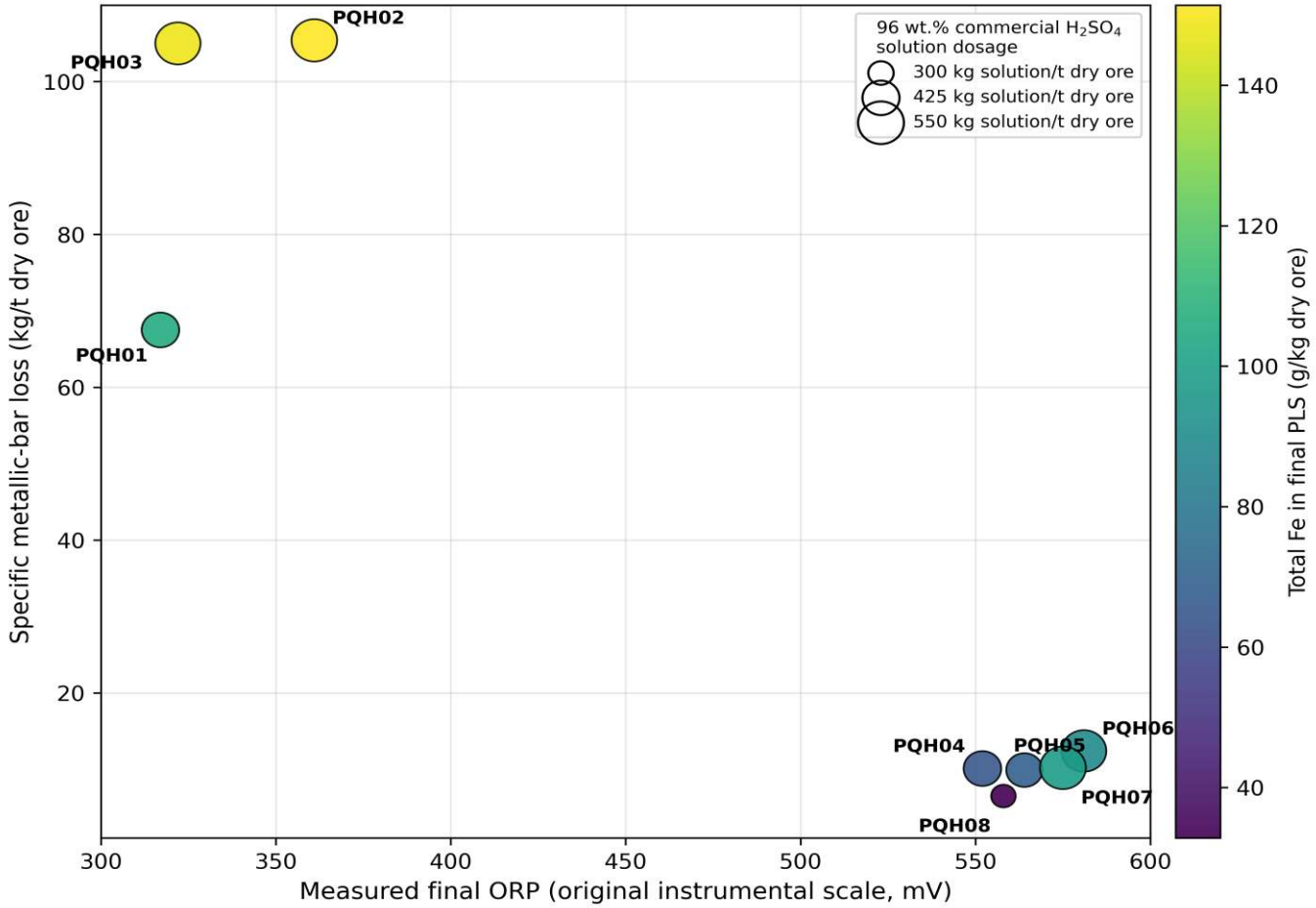


Figure 7. Specific metallic-bar loss as a function of measured final ORP, with total Fe loading shown by point color and dry-basis dosage of 96 wt.% commercial H_2SO_4 solution represented by bubble size. Source: Authors' calculations from the experimental mass and final-PLS data.

3.7. Recovered-solids-to-dry-feed ratio and residual Ni grade

Table 8 reports the recovered-solids-to-dry-feed ratio and final-residue Ni grade as descriptive mass-record indicators.

JIRRS
Journal International Review of Research Studies
Received: 28/06/2026 - **Accepted:** 23/07/2026
Vol: 01.10
DOI: 10.66104/xf9zhd03
Pages: 1-37

Table 8. Apparent recovered-solids-to-dry-feed ratio and final-residue Ni grade

Test	Recovered-solids-to-dry-feed ratio (%)	Difference from 100% (%)	Residual Ni (wt.%)
PQH01	91.35	8.65	0.65
PQH02	87.60	12.40	0.64
PQH03	82.59	17.41	0.64
PQH04	88.54	11.46	0.72
PQH05	86.46	13.54	0.73
PQH06	81.22	18.78	0.69
PQH07	83.71	16.29	0.62
PQH08	103.61	−3.61	0.77

Source: Authors' calculations from the experimental mass records and residue analyses.

PQH07 had the lowest residual Ni grade, whereas PQH08 retained more Ni in the solid. The apparent recovered-solids-to-dry-feed ratio of 103.61% for PQH08 indicates that the available mass records do not provide a physically closed solids balance. The result may reflect secondary precipitation, residual moisture, sample-handling differences, or inconsistencies among individual mass measurements. These ratios are retained only as process descriptors and are not used to quantify phase-specific dissolution.

3.8. Qualitative mineralogical transformation of final residues

Table 9 lists the selected normalized modal abundances measured in the final residues.

Table 9. Selected final-residue modal mineralogy (wt.%, normalized)

Test	Quartz	Verm./chl.	Serpentine	Altered Fe–Mg	Ni-bearing Si–Fe	Fe oxyhydroxides	Chromite	Mn oxides	Spinels
PQH01	8.95	1.00	0.72	0.57	24.08	47.84	14.18	0.00	0.09
PQH02	6.01	0.45	0.63	0.36	33.66	48.58	7.16	0.00	0.88
PQH03	9.05	0.93	0.77	0.44	20.32	45.94	19.55	0.00	0.07
PQH04	8.06	0.83	1.05	0.55	25.31	49.73	11.63	0.00	0.10
PQH05	8.95	1.07	0.95	0.45	24.97	44.10	17.08	0.00	0.11

JIRRS
Journal International Review of Research Studies
Received: 28/06/2026 - **Accepted:** 23/07/2026
Vol: 01.10
DOI: 10.66104/xf9zhd03
Pages: 1-37

Test	Quartz	Verm./chl.	Serpentine	Altered Fe–Mg	Ni-bearing Si–Fe	Fe oxyhydroxides	Chromite	Mn oxides	Spinels
PQH06	9.39	0.57	1.27	0.45	29.15	51.24	5.57	0.00	0.16
PQH07	9.48	0.52	0.57	0.33	24.82	46.93	15.09	0.00	0.09
PQH08	10.39	0.68	1.23	0.38	30.61	40.57	12.94	0.00	0.50

Source: Authors' compilation of the final-residue automated mineralogy data generated during the campaign.

The most consistent qualitative changes were strong modal depletion of vermiculite/chlorite and altered Fe–Mg silicates, variable but substantial depletion of serpentine, and persistence or residual enrichment of Fe oxyhydroxides, Ni-bearing Si–Fe plasma, quartz, chromite, and spinels. These trends are consistent with a lower relative modal contribution of Mg-bearing silicate phases and increasing dominance of ferruginous Ni hosts in the final residues (Araujo et al., 2026; Acquah et al., 2026; Kang et al., 2026). Modal increases in refractory phases do not imply mineral formation; they reflect normalization, selective depletion of other phases, and particle-scale heterogeneity. Because both feed and residue values are normalized modal proportions, apparent enrichment can result from depletion of other phases rather than mineral formation or an absolute mass increase.

Figure 8 compares the fixed 60:40 dry-mass-weighted reference feed with each final-residue modal distribution.

JIRRS
Journal International Review of Research Studies
Received: 28/06/2026 - **Accepted:** 23/07/2026
Vol: 01.10
DOI: 10.66104/xf9zhd03
Pages: 1-37

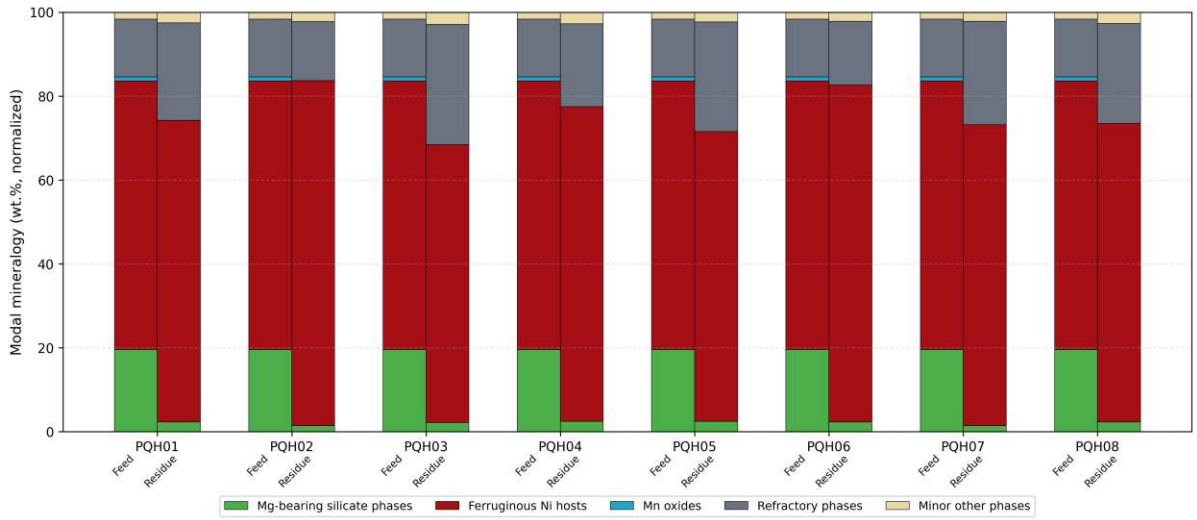


Figure 8. Fixed 60:40 dry-mass-weighted feed mineralogy and grouped final-residue mineralogy for PQH01–PQH08. Source: Authors' calculations using the nominal 60:40 dry-mass weighting and the automated-mineralogy data. Note. The comparison is qualitative; normalized modal enrichment may reflect depletion of other phases rather than mineral formation or absolute mass increase.

3.9. Mn oxides and the observed ORP–pH domain

Mn oxides were reported as not detected in every final residue, including those produced at measured final ORP values of 552–581 mV. The appropriate interpretation is that the Mn-oxide abundance was below the reporting limit of the automated mineralogy method. Complete dissolution cannot be claimed because the intermediate-residue mineralogy and a full Mn balance are unavailable. The numerical 0.00 entries therefore denote a below-reporting endpoint in normalized automated-mineralogy output, not a mass-balanced zero.

The below-detection endpoint was associated with final pH values of 0.58–1.09, temperatures of 94–98 °C, and positive residual acidity in the higher-ORP tests. These conditions form a provisional range observed in this campaign, not a minimum effective ORP or a validated operating window. The similarity of final-PLS Mn and Co yields between G1 and G3, together with the much lower bar consumption in G3, indicates that prolonged reduction was not associated with a proportional Mn or Co benefit. This interpretation is consistent with the known reactivity of Mn oxides and Co–Mn phases under acidic reducing conditions (Boassen et al., 2026; Domènech et al., 2022; Moro et al., 2023; Ziwa et al.,

JIRRS
Journal International Review of Research Studies
Received: 28/06/2026 - **Accepted:** 23/07/2026
Vol: 01.10
DOI: 10.66104/xf9zhd03
Pages: 1-37

2021). The observation is specific to this ore and campaign and should not be transferred as a universal ORP threshold.

3.10. Redistribution of residual Ni among mineral hosts

The relative contribution of Mg-bearing silicates and Mn oxides to mineralogically assigned Ni was lower in every final residue, whereas Fe oxyhydroxides and Ni-bearing Si–Fe plasma accounted for a larger share of residual Ni. These ferruginous hosts therefore dominated the residual mineralogical Ni inventory after the relative contribution of the Mg- and Mn-bearing groups decreased. Additional Ni mobilization from these hosts would likely increase total Fe transfer and downstream purification demand, consistent with the broader recovery–selectivity challenge reported for iron-rich laterites (da Silva Ribeiro et al., 2025; Hosseini Nasab et al., 2020; Ma et al., 2026; Prasetya et al., 2025). Figure 9 integrates the fixed 60:40 dry-mass-weighted feed and final-residue Ni-deportment distributions. This redistribution is relative and normalized; it does not constitute a mass-balanced measurement of phase-specific dissolution or absolute Ni removal from each host.

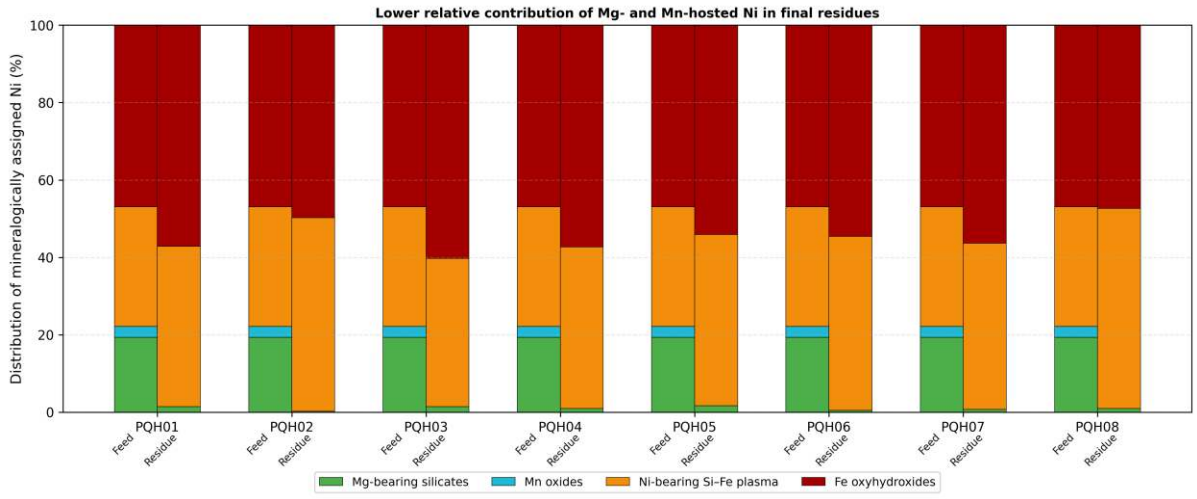


Figure 9. Redistribution of mineralogically assigned Ni among host groups from the fixed 60:40 dry-mass-weighted feed to the final residues of PQH01–PQH08. Source: Authors' compilation from the Ni-deportment data generated during the campaign. Note. Values represent normalized Ni

JIRRS
Journal International Review of Research Studies
Received: 28/06/2026 - **Accepted:** 23/07/2026
Vol: 01.10
DOI: 10.66104/xf9zhd03
Pages: 1-37

deportment; changes indicate relative redistribution among hosts and do not quantify phase-specific dissolution.

3.11. Defensible novelty and process implications

The defensible novelty is not causal optimization of acid dosage or redox potential. It is a screening-level operational comparison showing that prolonged metallic-bar exposure was associated with much greater metallic-material consumption and total Fe loading without a proportional increase in final-PLS Ni, Co, or Mn yield. The transferable contribution is the decision logic—evaluate valuable-metal yield together with Fe loading, reductant consumption, pH–ORP trajectory, and residue mineralogy—not the exact ORP, pH, or acid values observed for this ore. The data support development of controlled reductant dosing and full-stream monitoring but do not define a numerical industrial operating window. Reductant selection should be evaluated by electron efficiency, Fe addition, Co and Mn yield, safety, cost, and downstream compatibility (Moro et al., 2023; Santos & Schippers, 2023).

4. Study Limitations and Future Work

This screening-level operational study is supported by laboratory method codes, analytical techniques, dilution factors, and reporting limits. However, the instrument make/model and campaign-specific duplicate, certified-reference-material, and recovery summaries were not included in the PQH analytical package, and the ORP reference-electrode conversion was not reported. Commercial sulfuric acid containing 96 wt.% H_2SO_4 was used, with dosage expressed as commercial-solution mass per tonne of dry ore. Complete metallurgical balances could not be constructed because final-wash chemistry, solution retained in solids, and some process-loss information were unavailable. Consequently, only final-PLS yields are reported.

The campaign was not factorial: acid dosage, ORP, pH, metallic-bar exposure, solids concentration, ore mass, agitation, and stagewise acid distribution varied together. Approximate pairs with n = 2 provide only within-pair agreement. The mineralogy of the intermediate residue was not measured, so quantitative phase dissolution was removed from the revised analysis. The detection limit for Mn oxides was not documented. Total Fe

JIRRS
Journal International Review of Research Studies
Received: 28/06/2026 - **Accepted:** 23/07/2026
Vol: 01.10
DOI: 10.66104/xf9zhd03
Pages: 1-37

loading could not be partitioned between ore and bars. The observed associations are specific to one ore system and one campaign; external validity lies in the interpretive framework rather than in the numerical ORP, pH, or acid values.

Future work should use a controlled design with true triplicates, constant solids concentration and agitation, independently controlled pH and ORP on a known reference scale, a quantitatively dosed reductant, full balances of every liquor, wash, and solid, mineralogical sampling at intermediate and final times, and characterization of the reductant and corrosion products, Fe^{2+}/Fe^{3+} speciation, and blank metallic-bar corrosion tests. The +100 and −100 mesh fractions should be leached independently before any split-treatment flowsheet is proposed.

5. Conclusions

The PQH01–PQH08 campaign provides a screening-level operational comparison rather than a causal optimization. Dry-basis dosage of 96 wt.% commercial H_2SO_4 solution, measured ORP–pH trajectory, metallic-bar exposure, solids concentration, agitation, and mineralogy varied simultaneously, and the sequential procedure did not permit determination of an optimum acid split between size fractions. Metal responses were expressed as final-PLS yields per unit dry ore mass, not recovery or extraction. Three approximate n = 2 operational pairs were used only to describe within-pair agreement.

At nearly identical mean commercial-acid dosages of 543.6 kg solution/t dry ore for G1 and 543.3 kg solution/t dry ore for G3, the higher-ORP G3 operational bundle was associated with approximately 89% lower specific bar loss, 38% lower total Fe loading, 43% lower Fe/Ni, and 39% lower Fe/Co than G1. Final-PLS Co and Mn yields were similar, and there was no evidence of an important Ni yield penalty. The observed Ni difference was smaller than the within-pair variability of G3. The principal operational result is therefore the large reductant and total-Fe penalty associated with prolonged metallic-bar exposure, not an independently isolated ORP effect.

Final-residue mineralogy showed qualitative modal depletion of Mg-bearing silicates and concentration of residual Ni in Fe oxyhydroxides and Ni-bearing Si–Fe plasma. Mn-

JIRRS
Journal International Review of Research Studies
Received: 28/06/2026 - **Accepted:** 23/07/2026
Vol: 01.10
DOI: 10.66104/xf9zhd03
Pages: 1-37

oxide abundance was below the automated-mineralogy reporting limit in all final residues; this does not prove complete dissolution. The association is ore- and campaign-specific and does not establish a universal ORP threshold. The transferable contribution is a screening framework that combines final-PLS yield, total Fe loading, reductant consumption, ORP–pH trajectory, and qualitative residue mineralogy. A controlled follow-up campaign with complete balances, a known ORP scale, quantitative reductant dosing, independent pH control, Fe speciation, blank corrosion tests, and true replication is required before defining a validated operating window.

Declarations

Funding

This research received no external funding.

Conflicts of Interest

No conflict of interest is declared.

Data Availability

An anonymized supporting-data package may be made available through the editorial office upon reasonable request during peer review. Author-identifying access details will be restored after the double-blind review process. Full stream-balance data are not available for every test.

References

Abdollahi, H., Hosseini-Nasab, M., & Yadollahi, A. (2024). Bioleaching of lateritic nickel ores. In M. S. Hesami, A. Mousavi Khaneghah, & M. Soltani (Eds.), *Biotechnological innovations in the mineral-metal industry* (pp. 41–66). Springer Nature. https://doi.org/10.1007/978-3-031-43625-3_3.

Acquah, G., Abaka-Wood, G., Skinner, W., Addai-Mensah, J., & Asamoah, R. (2025). Effect of mechanical activation on nickel and cobalt extraction in refractory nickel laterite ore. Powder Technology, 468, 121655. https://doi.org/10.1016/j.powtec.2025.121655.

Acquah, G., Skinner, W., Abaka-Wood, G., Spiridonov, P., Addai-Mensah, J., & Asamoah, R. (2026). Extraction of nickel and cobalt from complex low-grade lateritic ores: Challenges and opportunities. *Minerals, 16*(3), Article 287. https://doi.org/10.3390/min16030287.

JIRRS
Journal International Review of Research Studies

Received: 28/06/2026 - **Accepted:** 23/07/2026
Vol: 01.10
DOI: 10.66104/xf9zhd03
Pages: 1-37

Araujo, F. P., Magalhães, N., Vassilieva, E., Rollinson, G., Andersen, J. C. Ø., Crane, R., Tampouris, S., Hughes, H. S. R., & Muchez, P. (2026). Mineralogical controls on Ni and Co recovery during HCl leaching of laterites. *International Journal of Minerals, Metallurgy and Materials, 33*(6). https://doi.org/10.1007/s12613-026-3396-7

Bafghi, M. S., Zakeri, A., Ghasemi, Z., & Adeli, M. (2008). Reductive dissolution of manganese ore in sulfuric acid in the presence of iron metal. Hydrometallurgy, 90(2–4), 207–212. https://doi.org/10.1016/j.hydromet.2007.07.003

Biswas, S. U., Karmakar, K., & Saha, B. (2021). Oxidation–reduction reactions in geochemistry. Vietnam Journal of Chemistry, 59(2), 133–145.

Boafo, K., Borkar, P., & Eisele, T. (2026). Overcoming the iron selectivity hurdle in nickel bioleaching: A critical review of mechanisms, economic challenges, and future research directions. *Mineral Processing and Extractive Metallurgy Review*. Advance online publication. https://doi.org/10.1080/08827508.2026.2638765.

Boassen, G. H. B., Zhu, M., Li, C., Luo, H., Wang, X., Liu, C., & Sun, J. (2026). Origin and structure of manganese oxides and their reactivity towards metal(loid)s. Reviews in Environmental Science and Bio/Technology, 25, Article 10.

Caetano, G. C., Ostroski, I. C., & Barros, M. A. S. D. (2025). Lateritic nickel and cobalt recovery routes: Strategic technologies. *Mineral Processing and Extractive Metallurgy Review, 46*(3), 400–414. https://doi.org/10.1080/08827508.2024.2328696.

Chi, D., Yu, J., Han, Y., Dong, Z., Gao, P., & Li, Y. (2026). Hydrometallurgical technologies of limonitic nickel laterite ore for carbon-neutral metallurgy: A review. JOM, 78(7), 6184–6210. https://doi.org/10.1007/s11837-026-08139-2

da Silva Ribeiro, G., de Deus Nascimento, N., da Silveira Ribeiro, R., de Paole Moreira Miranda, M., Martins, P. R., Costa Caetano, G., Alves de Andrade, L., & Ostroski, I. C. (2025). Optimization of the atmospheric acid leaching process for the recovery of nickel and cobalt from iron-rich lateritic ore. Mining, Metallurgy & Exploration, 42, 1127–1140.

de Alvarenga Oliveira, V., Rodrigues, M. L. M., & Leão, V. A. (2021). Reduction roasting and bioleaching of a limonite ore. Hydrometallurgy, 200, Article 105554.

Domènech, C., Villanova-de-Benavent, C., Proenza, J. A., Tauler, E., Lara, L., Galí, S., Soler, J. M., Campeny, M., & Ibáñez-Insa, J. (2022). Co–Mn mineralisations in the Ni laterite deposits of Loma Caribe (Dominican Republic) and Loma de Hierro (Venezuela). *Minerals, 12*(8), Article 927. https://doi.org/10.3390/min12080927.

Dong, B., Tian, Q., Xu, Z., Guo, X., Wang, Q., & Li, D. (2023). The effect of pre-roasting on atmospheric sulfuric acid leaching of saprolitic laterites. Hydrometallurgy, 218, Article 106063.

Gontijo, V. L., Teixeira, L. A. V., & Ciminelli, V. S. T. (2020). The reactivity of iron oxides and hydroxide during low-temperature sulfation. Hydrometallurgy, 197, Article 105452.

Hosseini Nasab, M., Noaparast, M., & Abdollahi, H. (2020). Dissolution optimization and kinetics of nickel and cobalt from iron-rich laterite ore, using sulfuric acid at atmospheric pressure. *International Journal of Chemical Kinetics, 52*, 283–298. https://doi.org/10.1002/kin.21349.

Hosseini Nasab, M., Noaparast, M., & Abdollahi, H. (2021). Direct and indirect bio-leaching of Co and Ni from an iron-rich laterite ore using Delftia acidovorans and Acidithiobacillus ferrooxidans. Journal of Mining and Environment, 12(2), 471–489.

Hosseini Nasab, M., Noaparast, M., & Abdollahi, H. (2022). Selective precipitation of iron from multi-element PLS produced by atmospheric leaching of Ni–Co-bearing laterite. International Journal of Mining and Geo-Engineering, 56(4), 309–313.

JIRRS
Journal International Review of Research Studies

Received: 28/06/2026 - **Accepted:** 23/07/2026
Vol: 01.10
DOI: 10.66104/xf9zhd03
Pages: 1-37

Huang, J., & Zhang, H. (2020). Redox reactions of iron and manganese oxides in complex systems. Frontiers of Environmental Science & Engineering, 14(5), Article 76.

Hussaini, S., Ozsarac, S., Ichlas, Z. T., Kursunoglu, S., & Kaya, M. (2025). Atmospheric leaching of a Turkish laterite in nitric acid solution. Journal of Mining Science, 61, 1014–1022.

Johnson, D. B., Smith, S. L., & Santos, A. L. (2021). Bioleaching of transition metals from limonitic laterite deposits and reassessment of the multiple roles of sulfur-oxidizing acidophiles in the process. Frontiers in Microbiology, 12, Article 703177.

Kang, H., Kim, J., & Kim, H.-J. (2026). Early-stage temperature-dependent leaching kinetics and mechanisms of saprolitic and limonitic nickel laterite ores under atmospheric conditions. *Minerals Engineering*, Article 110115. https://doi.org/10.1016/j.mineng.2026.110115.

Khan, S., Bhargav, P. K., Chaudhuri, M. G., Majumder, A., & Dey, R. (2026). Process optimization for selective nickel recovery from limonite ore using the Taguchi method. Minerals Engineering, 247, Article 110511.

Li, G., Chen, Y., Mang, C., Teng, X., Luo, J., & Rao, M. (2023). Near-zero-waste approach for the treatment of saprolitic nickel laterite via a combined hydrometallurgical process. *ACS Sustainable Chemistry & Engineering, 11*(18). https://doi.org/10.1021/acssuschemeng.2c05403.

Ma, H., Zhang, X., Wang, Y., Bai, P., Zhang, J., & Guan, M. (2026). Atmospheric sulfuric acid leaching of metals from nickel laterite and selective phosphate precipitation of $FePO_4$. Hydrometallurgy, 244, Article 106812. https://doi.org/10.1016/j.hydromet.2026.106812

McDonald, R. G., & Whittington, B. I. (2008). Atmospheric acid leaching of nickel laterites review: Part I. Sulphuric acid technologies. Hydrometallurgy, 91(1–4), 35–55. https://doi.org/10.1016/j.hydromet.2007.11.009

Moro, K., Haubrich, F., Martin, M., Grimmer, M., Hoth, N., & Schippers, A. (2023). Reductive leaching behavior of manganese and cobalt phases in laterite and manganese ores. Hydrometallurgy, 220, Article 106101.

Msumange, D. A., Jampaiah, D., Tardio, J., Nilsson, M., Arandiyan, H., & Bhargava, S. K. (2026). A review of nickel and cobalt from laterite ores: Toward sustainable extraction pathways for the battery industry. *Journal of Sustainable Metallurgy, 12*(2), 1038–1069. https://doi.org/10.1007/s40831-026-01439-6.

Mweene, L., Gomez-Flores, A., Jeong, H.-E., Ilyas, S., & Kim, H. (2024). Challenges and future in Ni laterite ore enrichment: A critical review. Mineral Processing and Extractive Metallurgy Review, 45(6), 539–563.

Pandey, N., Tripathy, S. K., Patra, S. K., & Jha, G. (2023). Recent progress in hydrometallurgical processing of nickel lateritic ore. *Transactions of the Indian Institute of Metals, 76*(1), 11–30. https://doi.org/10.1007/s12666-022-02706-2.

Pereira, A. C. (2026a). Mechanical activation in metallurgical processing: Mechanisms, applications and industrial perspectives. IKR Journal of Engineering and Technology, 2(2). https://doi.org/10.5281/zenodo.18912251

Pereira, A. C. (2026b). Balancing nickel recovery, iron dissolution, acid dosage, and residence time in atmospheric sulfuric acid leaching of a ferruginous lateritic nickel ore. Journal International Review of Research Studies, 1(9), 1–30. https://doi.org/10.66104/dempc459.

JIRRS
Journal International Review of Research Studies

Received: 28/06/2026 - **Accepted:** 23/07/2026
Vol: 01.10
DOI: 10.66104/xf9zhd03
Pages: 1-37

Prameswara, G., Amin, I., Ulfah, A. N., Trisnawati, I., Petrus, H. T. B. M., & Puspita, F. (2024). Atmospheric leaching behavior and kinetics study of roasted laterite ore. *Mining, Metallurgy & Exploration, 41*, 1025–1033. https://doi.org/10.1007/s42461-024-00947-x.

Prasetya, A., Putera, A. D. P., Sujoto, V. S. H., Zaidan, M. H., Abdurrahman, M. T., Andriani, A., Astuti, W., Sutijan, & Petrus, H. T. B. M. (2025). Enhanced recovery of nickel and cobalt from limonitic laterite ore: Optimization and kinetics of atmospheric sulfuric acid leaching. *Journal of Sustainable Metallurgy, 11*(4), 4127–4140. https://doi.org/10.1007/s40831-025-01231-y.

Ribeiro, P. P. M., dos Santos, I. D., Neumann, R., Fernandes, A., & Dutra, A. J. B. (2021). Roasting and leaching behavior of nickel laterite ore. *Metallurgical and Materials Transactions B, 52*(3), 1739–1754. https://doi.org/10.1007/s11663-021-02141-6.

Santos, A. L. A., Becheleni, E. M. A., Viana, P. R. M., Papini, R. M., Silvas, F. P. C., & Rocha, S. D. F. (2021). Kinetics of atmospheric leaching from a Brazilian nickel laterite ore allied to redox potential control. Mining, Metallurgy & Exploration, 38, 187–201. https://doi.org/10.1007/s42461-020-00310-w.

Santos, A. L., & Schippers, A. (2023). Reductive mineral bioprocessing. In D. B. Johnson, C. G. Bryan, M. Schlömann, & F. F. Roberto (Eds.), Biomining technologies: Extracting and recovering metals from ores and wastes (pp. 261–274). Springer.

Santos, A. L., Dybowska, A., Schofield, P. F., Herrington, R. J., & Johnson, D. B. (2020). Sulfur-enhanced reductive bioprocessing of cobalt-bearing materials for base metals recovery. Hydrometallurgy, 195, Article 105396.

Shayakhmetova, R., Mukhametzhanova, A., Osipov, P., Kali, A., Kuandykova, A., & Rakhym, A. (2025). Mechanism, kinetics and thermodynamics of nickel, iron, and magnesium hydrochloric acid leaching from laterite ore. *Scientific Reports, 15*, Article 41342. https://doi.org/10.1038/s41598-025-25276-x

Stanković, S., Goldmann, S., Kraemer, D., Ufer, K., & Schippers, A. (2024). Bioleaching of a lateritic ore (Piauí, Brazil) in percolators. Hydrometallurgy, 224, Article 106262.

Stanković, S., Kamberović, Ž., Friedrich, B., Stopić, S. R., Sokić, M., Marković, B., & Schippers, A. (2022). Options for hydrometallurgical treatment of Ni-Co lateritic ores for sustainable supply of nickel and cobalt for European battery industry from South-Eastern Europe and Turkey. *Metals, 12*(5), Article 807. https://doi.org/10.3390/met12050807

Stanković, S., Stopić, S., Sokić, M., Marković, B., & Friedrich, B. (2020). Review of the past, present, and future of the hydrometallurgical production of nickel and cobalt from lateritic ores. Metallurgical and Materials Engineering, 26(2), 199–208. https://doi.org/10.30544/513.

Tyassena, F. Y. P., Zuhud AL, M. D., Abrilla, A. M. A., Sarwana, W., Setyorini, D., Syafaatullah, A. Q., Ganing, M., Arninda, A., Rahim, H., & Prameswara, G. (2026). Optimizing microwave-assisted leaching of nickel from laterite ores: RSM-based modelling and kinetics. *Chemical Papers*. https://doi.org/10.1007/s11696-026-04911-5

Wang, K., Li, J., McDonald, R. G., & Browner, R. E. (2011). The effect of iron precipitation upon nickel losses from synthetic atmospheric nickel laterite leach solutions: Statistical analysis and modelling. Hydrometallurgy, 109(1–2), 140–152. https://doi.org/10.1016/j.hydromet.2011.06.009

Wang, Y., Wu, Y., Fan, Y., Wang, Y., & Li, L. (2024). Leaching kinetics of limonite-type laterite nickel ore from ammonium hydrogen sulfate solution at atmospheric pressure. JOM, 76(11), 6363–6375. https://doi.org/10.1007/s11837-024-06470-0.

JIRRS
Journal International Review of Research Studies

Received: 28/06/2026 - **Accepted:** 23/07/2026
Vol: 01.10
DOI: 10.66104/xf9zhd03
Pages: 1-37

Whittington, B. I., & Muir, D. (2000). Pressure acid leaching of nickel laterites: A review. Mineral Processing and Extractive Metallurgy Review, 21(6), 527–599. https://doi.org/10.1080/08827500008914177

Yunita, F. E., & Mubarok, M. Z. (2021). Nickel leaching from laterite ores by combination of organic and sulfuric acid. *AIP Conference Proceedings, 2382*(1), Article 050003. https://doi.org/10.1063/5.0060750.

Zablotskaya, Y. V., Sadykhov, G. B., Anisonyan, K. G., Smirnova, V. B., & Tuzhilin, A. S. (2022). On the problem of enhancing selectivity of nickel and cobalt recovery during the sulfuric acid leaching of reduced oxidized nickel ore. Russian Metallurgy (Metally), 2022(9), 985–989. DOI: 10.1134/S0036029522090142.

Zhang, P., Guo, Q., Qu, J., & Qi, T. (2020). Leaching Ni and Co from saprolitic laterite ore by employing atmospheric acid leaching solution with high concentration of $FeCl_3$ at mild conditions. Russian Journal of Non-Ferrous Metals, 61, 42–48.

Ziwa, G., Crane, R., & Hudson-Edwards, K. A. (2021). Geochemistry, mineralogy and microbiology of cobalt in mining-affected environments. Minerals, 11(1), Article 22.